TOC

Suppression of Autofluorescence based on Fuzzy Classification by Spectral Angles

Milan Gavrilovic[1], Carolina Wählby[1,2]

[1] Centre for Image Analysis, Uppsala University, Box 337, SE-75105 Uppsala, Sweden
{milan,carolina}@cb.uu.se
[2] currently at the Broad Institute of Harvard and MIT, 7 Cambridge Center, MA 02142

Abstract. Background fluorescence, also known as autofluorescence, and cross-talk are two problems in fluorescence microscopy that stem from similar phenomena. When biological specimens are imaged, the detected signal often contains contributions from fluorescence originating from sources other than the imaged fluorophore. This fluorescence could either come from the specimen itself (autofluorescence), or from fluorophores with partly overlapping emission spectra (cross-talk). In order to resolve spectral components at least two distinct wavelength intervals have to be imaged. This paper shows how autofluorescence can be presented statistically using a spectral angle histogram. Pixel classification by spectral angles was previously developed for detection and quantification of colocalization. Here we show how the spectral angle histogram can be employed to suppress autofluorescence. First, classical background subtraction (also referred to as linear unmixing) is presented in the form of a fuzzy classification by spectral angles. A modification of the fuzzy classification rules is also presented and we show that sigmoid membership functions lead to better suppression of background and amplification of true signals.

Keywords: autofluorescence, fluorescence microscopy, multispectral image analysis, fuzzy classification, dimensionality reduction

1 Introduction

Autofluorescence, i.e., fluorescence from other substances than the fluorophores of interest, can be limited either chemically while specimens are prepared or during the imaging by using appropriate filter and microscope settings. Autofluorescence can also be suppressed by image analysis based methods, traditionally by spectral unmixing in the same fashion as cross-talk suppression [1, 2, 3]. In recent years, autofluorescence removal has been treated as a blind spectral decomposition problem solved by multispectral imaging [4, 5].

In this paper we address how autofluorescence can be presented statistically from as few as two spectral channels using a spectral angle histogram [6]. We also show how the parameters needed for background subtraction can be extracted from a

spectral angle histogram. Unlike 2D histograms or scatterplots, commonly used for representation of the relationship between two channels, spectral angle histograms describe the same relationship with the dimensionality reduced to one. Automated analysis of one-dimensional histograms in general is more convenient as standard methods for histogram segmentation can be applied. Specifically, analysis of the shape of a 1D spectral angle histogram can provide input parameters both for linear unmixing (e.g., background subtraction) and the novel method proposed in this paper.

In many cases, it is of interest to limit the amount of image data that has to be collected, and we show that autofluorescence can be suppressed using only two channels, one showing both fluorescent signals and background, and one showing only background fluorescence (see Fig.1). In this paper, we will follow a convention in fluorescence microscopy and associate ratios between two pixel values with hues in the dual colour image. A pixel that represents a true signal should have a higher ratio of "red" to "green" values than a pixel that belongs to the background. Naturally, "red" and "green" could be any pair of wavelength intervals representing signal and autofluorescence.

2 Background

2.1 Background subtraction

Background subtraction, also referred to as linear unmixing [7], is a classical method for suppression of autofluorescence and cross-talk. It reduces to simple subtraction in cases when one channel has contributions from two sources of fluorescence (i.e., signals and background in the "red" channel R) and the other channel has contribution from the background (i.e., background imaged in the "green" channel G). The autofluorescence compensated channel R_{comp} containing only true signals is calculated using (1) where s depends on the ratio of intensities in channels R and G.

$$R_{comp,B.S.} = \max(0, R - s \cdot G) \quad \textbf{(1)}$$

Methods described in this paper can be used for suppression of autofluorescence in general, although they are designed for the more difficult problem in which signals are sparsely scattered over the background as seen in Fig.1. The relationship between the two channels is shown in Fig.2. Here, any algorithm that searches for the ratio of intensities in channels R and G associated with the true signals would give unstable results. As seen in the 2D histogram of Fig.2B, the image is dominated by a ratio of intensities equal to k_0 which shows that the two channels as almost linearly dependent. On the other hand, the scatterplot in Fig.2B shows a group of ordered pairs (R,G) that represents the true signals.

If the parameter s needed for equation (1) is calculated using Principal component analysis or a similar method, the first component is located around the line $G=k_0 \cdot R$, where k_0 is the median ratio of intensities. Using $s=k_0^{-1}$ results in somewhat suppressed background, but still does not give the optimal result as most of the background intensity levels in R are still greater than zero. Therefore, parameter s should be smaller than k_0^{-1} in order to suppress all the bright pixels associated with the

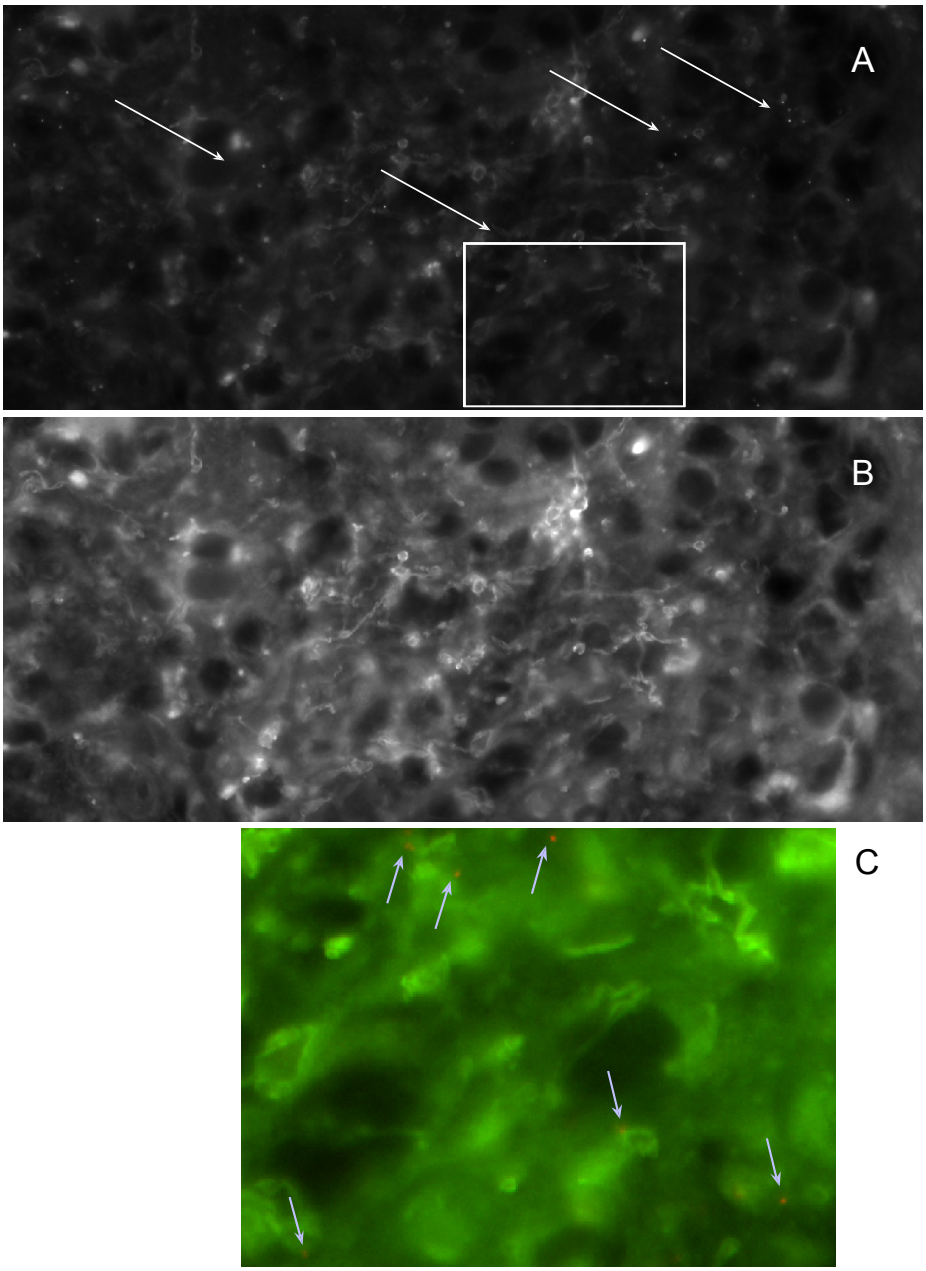

Fig.1. Tissue section showing: (**A**) Alexa555 labeled FISH probes excited at 563nm (the "red" channel); (**B**) Lipofuscin and hemoglobin autofluorescence imaged using the FITC channel (excited at 488nm, the "green" channel) where the Alexa555 signal is not seen. (**C**) Zoom in on A, the combined image. The arrows point at a few true signals. These signals are visible as red and orange blobs over yellow-green background. The white rectangle shows the area that is used in Section 5 to compare the described methods visually.

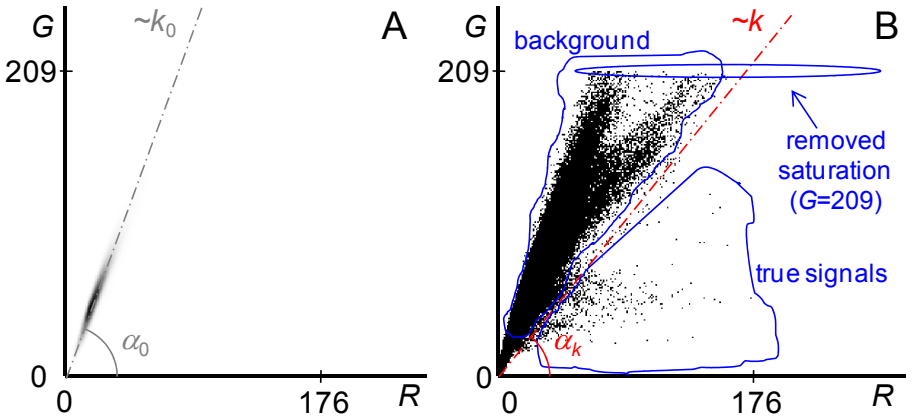

Fig.2. (A) In a 2D histogram of the red (Fig.1A) against the green (Fig.1B) channel, the darker regions represent the more common ordered pairs (R,G), and only the dominating pairs corresponding to background fluorescence are visible. **(B)** In a scatterplot of the same data, each type of ordered pairs (R,G) is represented by a black point, independent of the number of pairs. Here it is possible to see the red-green pairs of the true signals as they deviate from the large cluster representing background fluorescence.

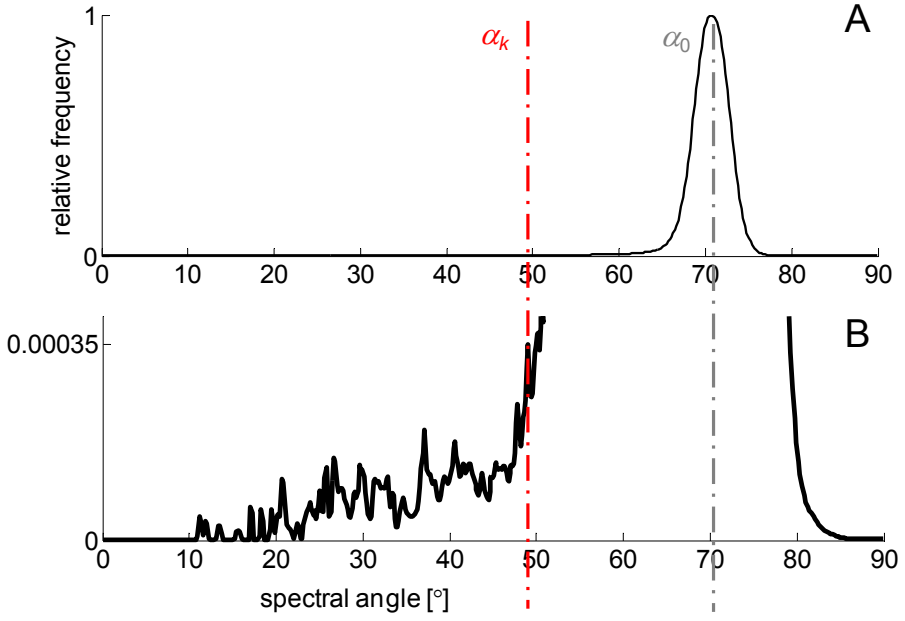

Fig.3. (A) Spectral angle histogram showing relative intensity distribution over the range of spectral angles, where 0° represents "pure red" and 90° represents "pure green". Background fluorescence is visible as a strong and smooth peak at α_0. **(B)** The histogram zoomed 3000 times in ordinate axis showing weak signals represented by a series of local maxima in the range of spectral angles between 0° and α_k.

background. Calculating the principal component associated with the true signals will not give stable results due to the small number of true signals present.

2.2 Spectral angles and angle histograms

An image consisting of two colour channels, can be thought of as a collection of pixel samples (R,G) from a colour spectrum varying from red to orange to yellow to yellowish green to green. The spectral angle can be described by the angular deviation of the pixel (R,G) from the red intensity axes of a scatterplot. An angle histogram, calculated using the infinity norm of (R,G) as a weight and compensated for quantification noise, is simply a histogram where each bin represents a given angle interval [6].

Here, we reduce the 2D histogram of Fig.2 to a 1D angle histogram, and extract the parameter k based on the histogram shape as described below. A spectral angle histogram can be useful for both automated background subtraction and for generation of more general fuzzy classification rules. The angle histogram that corresponds to the 2D data representation in Fig.2 is shown in Fig.3. Saturation in the channel G should be avoided during the image acquisition as it results in false spectral angles. If saturation is present, saturated pixels should be excluded, as it is impossible to extract useful information from them.

3 Methods

3.1 Background subtraction as a fuzzy membership function

Equation (1) describes how an autofluorescence compensated image R_{comp} containing only true signals, can be calculated. The parameter s should be associated with the slope of the line $G=k\cdot R$ shown in the scatterplot in Fig.2B. If a spectral angle α is defined as $\alpha=\arctan(G/R)$, the spectral angle α_k of that line is given by $\alpha_k=\arctan k=\arctan s^{-1}=90°-\arctan s$. Thus, equation (1) can be rewritten as shown in equation (2). The second term in equation (2) has the form of a fuzzy membership function of the spectral angle α. Therefore, background subtraction can be considered as a special case of generating a fuzzy classification by spectral angles with a tangent membership function.

$$\begin{aligned} R_{comp,B.S.} &= \max(0, R - s\cdot G) \\ R_{comp,B.S.} &= \max\left(0, R\cdot\left(1 - s\cdot\frac{G}{R}\right)\right) \\ R_{comp,B.S.} &= R\cdot\max\left(0, 1-\tan(90°-\alpha_k)\cdot\tan\alpha\right) \end{aligned} \quad \textbf{(2)}$$

3.2 Nonlinear unmixing: the sigmoid membership function

As the photons recorded in the "red" channel come from fluorophores representing both the signals and the background fluorescence, and there are no nonlinear

phenomena that should be modeled, a linear combination of the "red" and the "green" channels is the only physically correct approach to produce the image R_{comp} showing only signals. On the other hand, for the purpose of detection and quantification of the number of objects we are interested in amplifying intensities of the pixels representing true signals, e.g., no matter whether the spectral angle is 0° or close to α_k. That is not possible if subtraction is used since pixels with higher spectral angles are more suppressed for every choice of α_k. Therefore, a sigmoid membership function (3) is a natural choice providing a soft pixel classification by spectral angles. The proposed function is commonly used for fuzzy thresholding [8].

$$R_{comp,sigm} = R \cdot \max\left(0{,}1 - \frac{1}{1+\exp(-p\cdot(\alpha-\alpha_c))}\right) \quad (3)$$

The parameter α_c is associated with the highest spectral angle representing the signal, with membership value equal to 0.5, and p is used for scaling the sigmoid function.

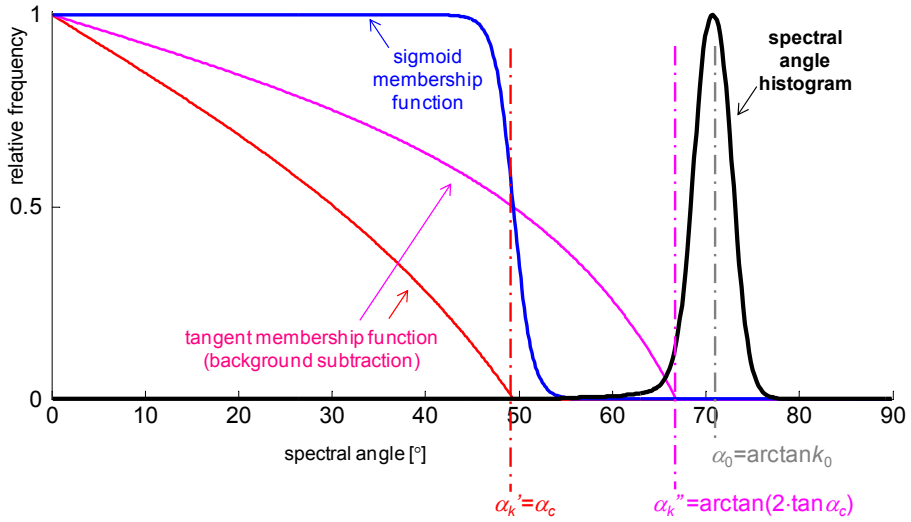

Fig.4. The angle histogram shown in Fig.3 is used for tuning the parameters α_k and α_c needed for equations (2) and (3), respectively. Both types of membership functions suppress spectral angles classified as background to 0, and leaves spectral angles associated with the true signals.

3.3 Defining membership function parameters

Parameter α_c can be extracted by assuming that α_0 is the peak associated with the background, i.e., the angle at the maximum value in the angle histogram, and α_c is determined by the last local maximum in the series of local maxima between 0° and α_0. For automatic calculation of α_c, the original angle histogram is smoothed by a series of Gaussian filters with standard deviation σ ranging from zero to eight. For each σ the last local maximum of the smoothed angle histogram in the range 0 to α_0 is

detected. Thereafter α_c is set to the average value of all last local maxima, increasing robustness. Pixels with spectral angles greater than α_c should be classified as background, and thus the fuzzy membership function should have values close to 0 in that range, and pixels with spectral angles lower than α_c are associated with the true signals, i.e., the membership function should be significantly greater than 0 in that range. Parameter p is typically set to one. Such a sigmoid membership function is shown in Fig.4.

The same method is used for extraction of the background subtraction parameter α_k. Unlike the sigmoid function, the tangent membership function shown in equation (2) is more rigid. The position of the peak α_c can be used either to suppress the content to the right of the peak completely ($\alpha_k'=\alpha_c$) or to 50% of its value just like the sigmoid membership function: $0.5=1-\tan(90°-\alpha_k'')\cdot\tan\alpha_c \Rightarrow \alpha_k''=\arctan(2\cdot\tan\alpha_c)$.

4 Materials

4.1 Image data

Images used for testing the presented methods come from a study of protein complex formation in brain tissue. Brain tissue is highly autofluorescent due to the presence of lipofuscin and hemoglobin. Protein complexes are detected using the proximity ligation assay [9], where each detection event gives rise to a concatemeric DNA strand that folds into a micrometer sized coil, detected by Alexa555 labeled FISH probes excited at 563nm. Lipofuscin and hemoglobin fluorescence have very broad spectral profiles and are imaged using the FITC channel (excited at 488nm) where the Alexa555 signal is not seen. The image stacks are 1288x1024x30 voxels in size with signals distributed over a number of slices.

To guarantee a fair comparison of the presented methods, a test set of 69 images acquired under the same conditions was randomly selected.

4.2 Ground truth generation

The complete image analysis of the material could be provided even without background suppression. Signals are small, bright and always have regular Gaussian shape meaning that the true signals are detected by careful shape modeling. To generate the ground truth used for comparison of the methods described in section 3, we produce binary 2D masks of signals by using the so called Stable Wave Detector [10].

5 Results

Before either the 2D histogram or the spectral angle histogram was created, the data was shifted by subtracting the minimum intensity values in both channels separately. This corrected for the microscope intensity offset. Using similar dynamic range is not

essential, though the methods were tested for data sets with k_0 varying from one to six (e.g., in the example shown in Fig.2A, k_0=2.9). The plots shown in Fig.2-4 represent the relationship between the two channels of one of the test images (see Fig.1) from the set described in section 4.1. The strongest peak in Fig.3 and Fig.4 at k_0=71° clearly shows that the expected range of the spectral angles representing autofluorescence is associated with the peak.

For the sigmoid membership function α_c was determined to 49.4°. For the tangent membership function the parameter for background subtraction α_k' was set to α_c=49.4°, a reasonable choice for both methods since ordered pairs (R,G) of pixels representing signals are left on one side of the line $G=k\cdot R$, where $k=\tan\alpha_k$', and pairs representing the background on the other side of the line (see the scatterplot in Fig.2B). The one-dimensional intensity profiles in Fig.5 show the difference between background subtraction using the tangent membership function, and fuzzy classification using the sigmoid membership function. Signals close to α_c are more suppressed by background subtraction than by the sigmoid membership function. Although the sigmoid transformation is not linear, it will improve the result of the study as a larger number of signals can be enhanced, and thereby improve recall of signal counts.

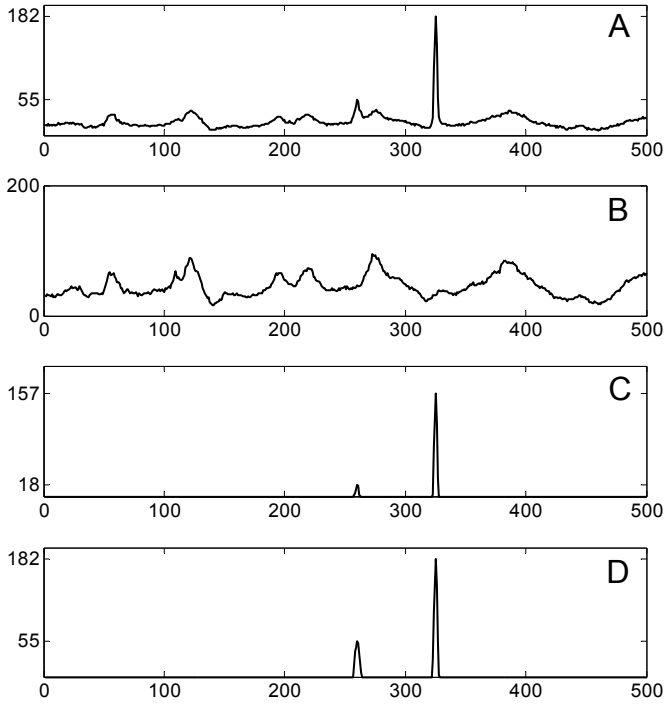

Fig.5. Intensity distribution over one spatial dimension taken from an image in the data set described in Section 4.1 showing: **(A)** two signals over the background (one weak and one strong); **(B)** background; **(C)** the result of background subtraction, i.e., linear unmixing or fuzzy classification using the tangent membership function; **(D)** the result of fuzzy classification as defined in equation (5), using the sigmoid function, i.e., nonlinear unmixing.

5.1 Comparison

In Section 3 we discussed unmixing methods – nonlinear unmixing (or fuzzy classification using the sigmoid membership function centered at α_c) and linear unmixing, that can be implemented either as background subtraction determined by α_k'=α_c, or background subtraction determined by α_k"=arctan(2·tanα_c). In addition, we compared these methods with signal enhancement using a simple morphological top-hat filter. The top-hat filtering was applied to the "red" Alexa 555 image. A background image is created by opening the input image with a non-flat structuring element with the origin in its centre. Thereafter, the background image is subtracted from the input to yield an enhancement of the signals as defined in (4). The structuring element is modeled by the shape of a signal (i.e., values are chosen to match an average 3x3 size signal).

$$R_{comp,M.O.} = R - R \circ SE, \quad SE = \frac{1}{28}\begin{bmatrix} 5 & 15 & 5 \\ 15 & 28 & 15 \\ 5 & 15 & 5 \end{bmatrix} \tag{4}$$

A very common method for background suppression, surface fitting, was not used or tested due to irregular variations of the background [11].

Since images R_{comp} produced by the four described methods have different intensity ranges, a fair comparison of the methods was guaranteed by fixing the "optimal" threshold to the intensity where exactly one false positive was detected (see value 1 in Fig.6). Finally, Fig.6 shows the result on the 69 test images. The left plot shows that both the sigmoid membership function and background subtraction with α_k'=49.4° keep the number of false positives low (i.e., high precision). For such range of the intensity thresholds, recall is relatively low for all four methods, although the sigmoid membership function and background subtraction with α_k"=66.8° have the highest recall values (i.e., true positive rate). Therefore, we conclude that the sigmoid membership function gives similar result to that of the tangent membership function with low α_k considering suppression of false signals, and similar or even better result than the tangent membership function with high α_k considering amplification of true signals.

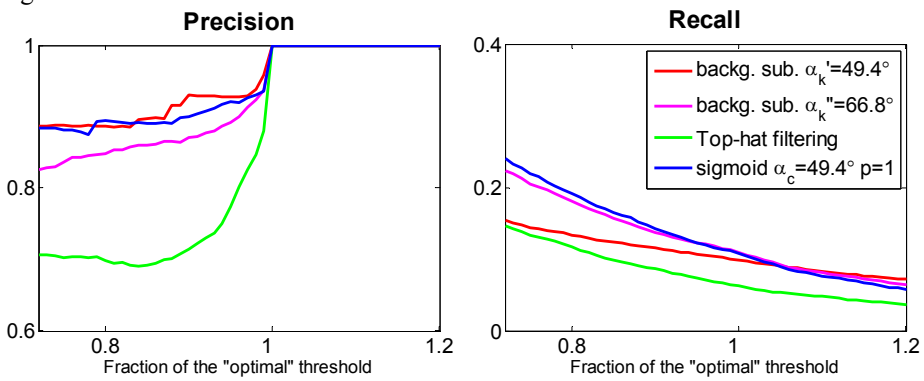

Fig.6. Plots show precision and recall of each of the four methods applied to the image test set described in section 4.

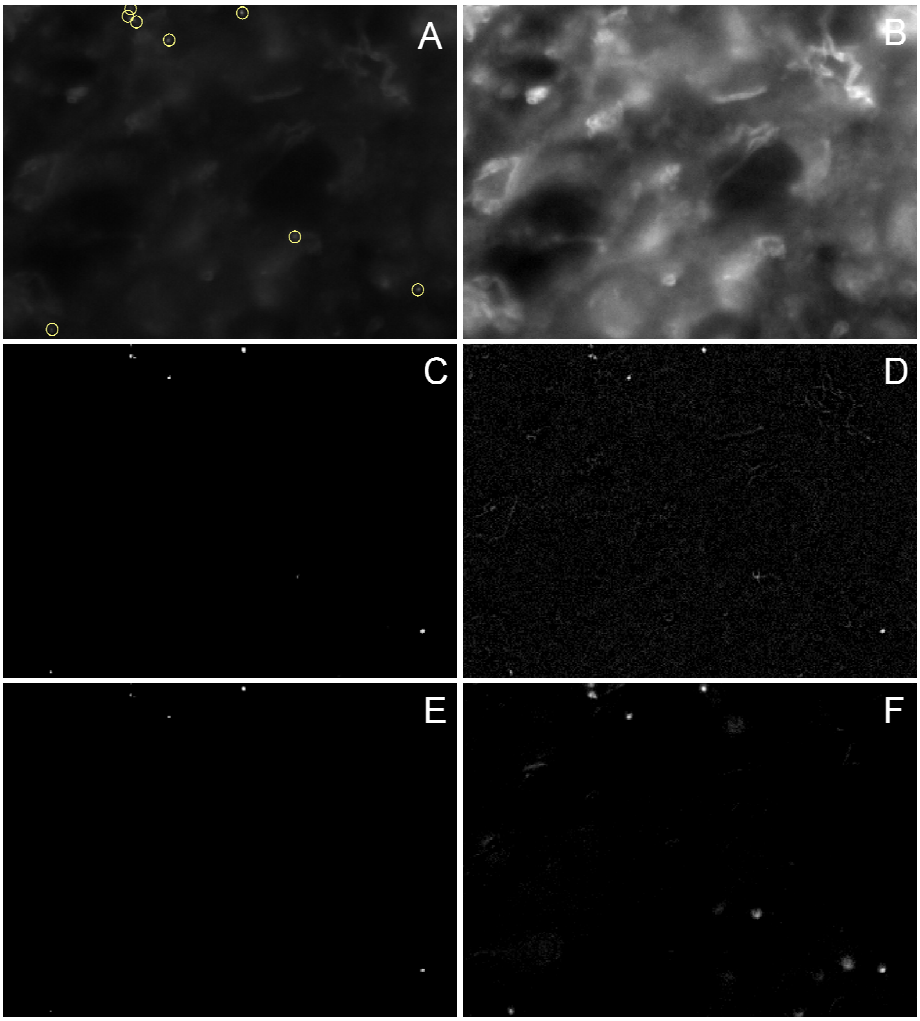

Fig.7. (A) Red channel of the part of the image shown in Fig.1. Circles denote the ground truth. **(B)** Corresponding autofluorescence image. **(C)** The result of fuzzy classification (α_c=49.4° and p=1) shows bright signals and flat background. **(D)** Top-hat filtering results in a non-flat background as it also enhances some of the structures in the auto-fluorescent tissue. **(E,F)** The results of background subtraction with α_k'=α_c=49.4° (E) and α_k"=arctan(2tanα_c)=66.8° (F) show either weaker signals than fuzzy classification using the sigmoid membership function or artifacts in the background. Images (C)-(F) are scaled to cover the full dynamic range and log transformed to visualize the variations in signal to background achieved with the different methods.

Results produced by another choice of "optimal" threshold are shown in Table 1. For each image, the "optimal" threshold was determined by the maximal value of the F_1-score. Precision and recall were calculated for all 69 images in the test set that had more than one signal detected giving mean values and standard deviations of

precision and recall. The previous conclusion is confirmed as the method based on fuzzy classification using the sigmoid membership function has the highest precision value when compared to the ground truth, together with linear unmixing that completely suppresses the background (α_k'=α_c). With a higher value of α_k', the precision was lower, though the recall was higher. On the other hand, the simple top-hat filtering described by equation (4) had the highest recall value. This was expected because the "ground truth" was created by a similar, more advanced, shape-based algorithm. Finally, the high signal-to-noise ratio of the first two methods gave visually more appealing results as shown in Fig.7.

Table 1. Mean values and standard deviations of precision and recall of the same image data used to generate Fig.6 with another choice of the "optimal" threshold, followed by signal-to-noise ratio.

	Precision		Recall		SNR
Methods:	*mean*	*std*	*mean*	*std*	
Sigmoid (α_c=49.4°, p=1)	0.85	0.12	0.51	0.15	75
Backg. sub. (α_k''=66.8°)	0.66	0.20	0.58	0.17	24
Backg. sub. (α_k'=49.4°)	0.83	0.15	0.43	0.14	70
Top-hat filtering	0.65	0.18	0.65	0.18	17

6 Conclusions and further development

Although the proposed algorithm is of higher complexity than simple background subtraction, these methods have shown to be useful (M. Jarvius, Dept. of Genetics and Pathology, Uppsala University, *personal communication*). By using the described methods it was possible to tune the parameters of the fuzzy classification rules and apply them on a large data set that consists of thousands of two-channel images that were not acquired with the constrains required for correct linear unmixing [7]. In spite of the high complexity of parameter extraction, time was saved in image acquisition when compared to multispectral imaging solutions, which require a large number of channels to be recorded. Also, storage of multispectral images is unnecessary since only one channel showing the signals and one channel showing background are required.

Development of more robust algorithms for parameter extraction is a challenge. For instance, if image data was not disrupted by saturation, the background cluster would follow the normal distribution allowing us to determine α_c by placing the angle threshold at certain standard deviation. Finally, if the number of signals was larger, the spectral angle histogram would be bimodal. In that case α_c could be determined by an algorithm that searches for a minimum between the two peaks.

Spectral angle histograms can be used for extraction of the parameters for cross-talk suppression, but also for generation of fuzzy classification rules that would amplify each fluorophore without changing the original intensity values as done by linear unmixing. As the proposed method performs pixel classification, it is independent of the spatial and time resolution of the image data, and thus directly applicable to 3D images or time-sequences. All described algorithms were

implemented in Matlab (The MathWorks, Inc., Natick, MA), and are available from the authors on request for research purposes.

Using fuzzy classification rules in general can be considered as nonlinear unmixing, preserving the original intensities of the signals of interest, but affecting the shape of the resulting objects. In such situations, the method can provide masks for fuzzy segmentation or classification, but should be used with care as a substitute for classical linear unmixing in quantitative analysis of biological data.

Acknowledgments. This project was funded by the EU-Strep project ENLIGHT (ENhanced LIGase based Histochemical Techniques). The authors would like to thank Ewert Bengtsson and Cris Luengo at the Centre for Image Analysis in Uppsala for fruitful discussions regarding the methods. The authors would also like to thank Malin Jarvius at the Department of Genetics and Pathology, Uppsala University, for kindly providing the image data.

7 References

1. Carlsson, K., Mossberg, K.: Reduction of cross-talk between fluorescent labels in scanning laser microscopy. Journal of Microscopy 167(1), 23-37 (1992)
2. Patwardhan, A., Manders, E. M. M.: Three-colour confocal microscopy with improved colocalization capability and cross-talk suppression. Bioimaging 4, 17-24 (1996)
3. Luengo Hendriks, C. L., Keränen, S. V. E., Biggin, M. D., Knowles, D. W.: Automatic channel unmixing for high-throughput quantitative analysis of fluorescence images. *Optics Express* 15(19), 12306-12317 (2007)
4. Dickinson, M.E., Bearman, G., Tille, S., Lansford, R., Fraser, S.E.: Multi-Spectral Imaging and Linear Unmixing Add a Whole New Dimension to Laser Scanning Fluorescence Microscopy. BioTechniques 31(6), 1272-1278 (2001)
5. Mansfield, J.R., Gossage, K.W., Hoyt, C.C., Levenson, R.M.: Autofluorescence removal, multiplexing and automated analysis methods for in-vivo fluorescence imaging. Journal of Biomedical Optics 10(4), 041207 (2005)
6. Gavrilovic, M., Wählby, C.: Quantification of colocalization and cross-talk based on spectral angles. Journal of Microscopy 234(3), 311-324 (2009)
7. Zimmermann T.: Spectral Imaging and Linear Unmixing in Light Microscopy. In: *Advances in Biochemical Engineering / Biotechnology*, Springer-Verlag, Berlin-Heidelberg, vol. 95, pp. 245-265 (2005)
8. Pal, S.K., Rosenfeld, A.: Image enhancement and thresholding by optimization of fuzzy compactness. Pattern Recognition Letters 7(2), 77-86 (1998)
9. Söderberg O., Gullberg M., Jarvius M., Ridderstråle K., Leuchowius K-J., Jarvius J., Wester K., Hydbring P., Bahram F., Larsson L-G., Landegren, U.: Direct observation of individual endogenous protein complexes *in situ* by proximity ligation. *Nature Methods* 3(12), 995–1000 (2006)
10. Dupac J, Hlavac V.: Stable wave detector of blobs in Images. In: 28th Annual Symposium of the German Association for Pattern Recognition (DAGM), Berlin, 2006. LNCS, vol. 4174, pp. 760–769. Springer Verlag (2006)
11. Wu, Q., Merchant, F. A., Castleman, K. R.: Microscope Image Processing. Elsevier Inc. Oxford, UK (2008)